Supplement of Geosci. Model Dev. Discuss., 8, 6217–6266, 2015
http://www.geosci-model-dev-discuss.net/8/6217/2015/
doi:10.5194/gmdd-8-6217-2015-supplement

Geoscientific Model Development Discussions
Open Access

Supplement of

A global scale mechanistic model of the photosynthetic capacity

A. A. Ali et al.

Correspondence to: C. Xu (xuchongang@gmail.com)

Supplementary Figures

Figure S1 Convergence of parameters obtained by using the Differential Evolution Adaptive Metropolis Snooker updater (DREAM-ZS) sampling technique when TRF1 (temperature acclimation was assumed in the model) was used. The parameters include par1: J_{maxb0} (unitless) is the baseline proportion of nitrogen allocated for electron transport rate; par2: J_{maxb1} (unitless) determines the electron transport rate response to light; par3: t_{c,j_0}(unitless) is the baseline ratio of rubisco limited rate to light limited; and par4: H (unitless) determines electron transport rate response to relative humidity. The vertical axis (R_{stat}) represents the deviance of model prediction from observations.

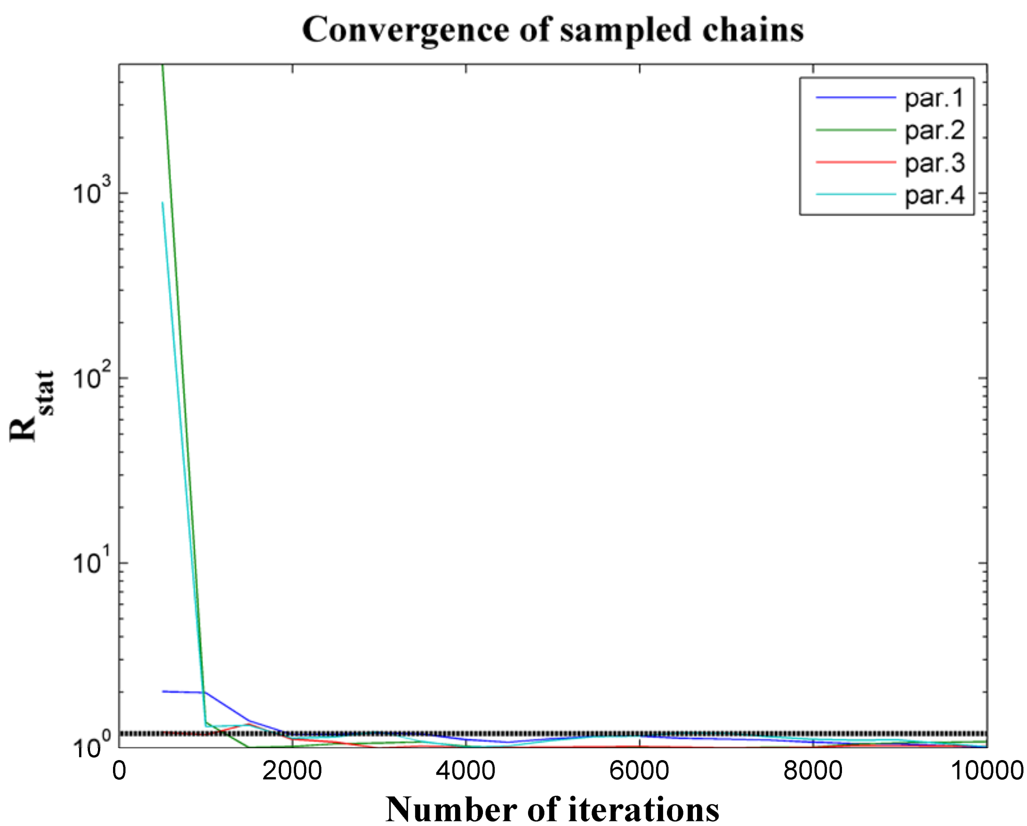

Figure S2 Convergence of parameters obtained by using the Differential Evolution Adaptive Metropolis Snooker updater (DREAM-ZS) sampling technique when TRF2 (temperature acclimation was not assumed in the model) was used. The parameters include par1: J_{maxb0} (unitless) is the baseline proportion of nitrogen allocated for electron transport rate; par2: J_{maxb1} (unitless) determines the electron transport rate response to light; par3: t_{c,j_0}(unitless) is the baseline ratio of rubisco limited rate to light limited; and par4: H (unitless) determines electron transport rate response to relative humidity. The vertical axis (R_{stat}) represents the deviance of model prediction from observations.

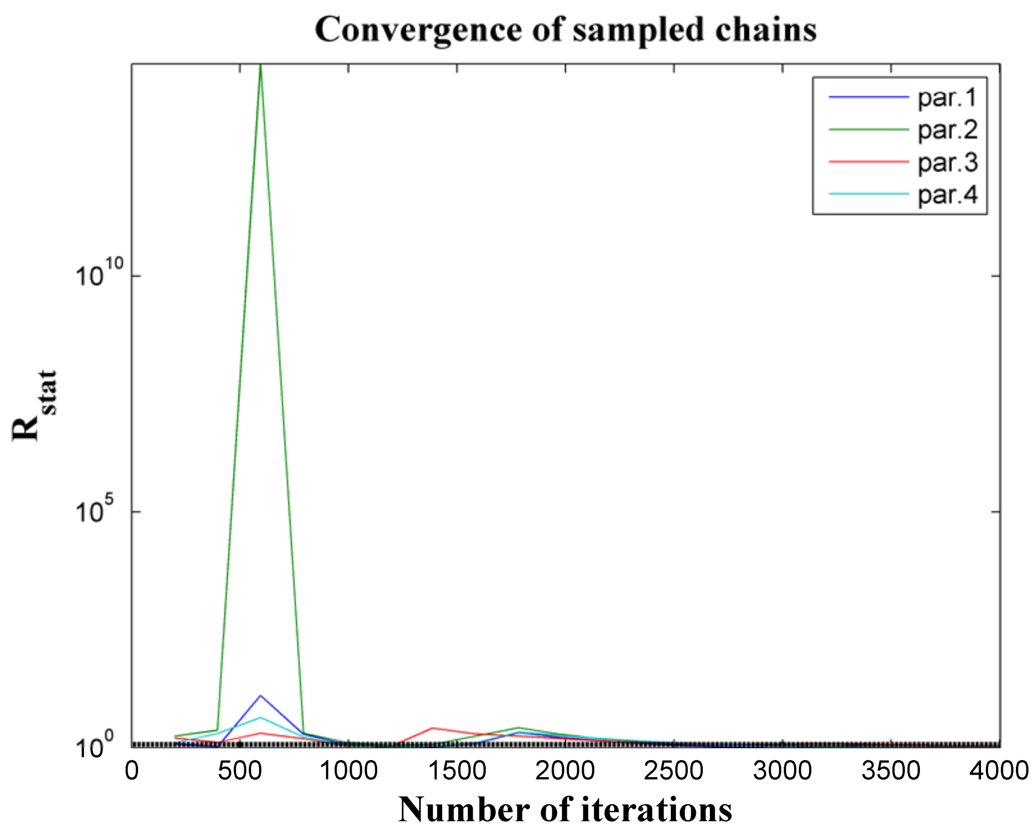

Figure S3 Percentage of variations (r^2, ME; model efficiency) in observed $V_{c,max25}$ (μmol CO_2 m^{-2} s^{-1}) explained by modeled $V_{c,max25}$ (a, c) and in observed J_{max25} (μmol electron m^{-2} s^{-1}) explained by modeled J_{max25} (b, d) across the growing season. The nitrogen allocation model was run with the environmental variables, leaf mass per leaf area, and the leaf nitrogen contents by using either TRF1 (a, b) or TRF2 (c, d). TRF1 was a temperature response function that considered the potential for acclimation to growth temperature while TRF2 was a temperature response function that did not consider change in temperature response coefficients to growth temperature. The r^2 is derived by a linear regression between observed and modeled values. All of the studies that considered $V_{c,max}$ and J_{max} measurements across the growing season were considered.

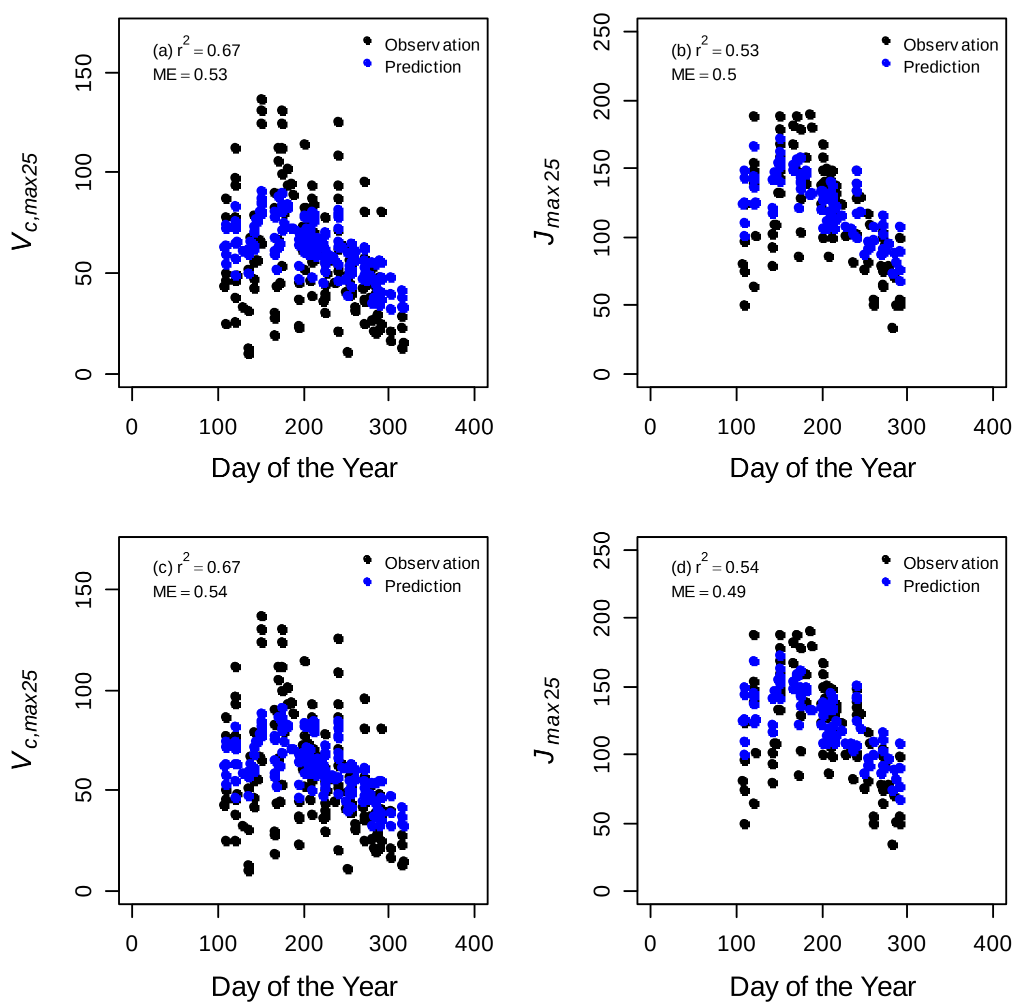

Figure S4 Percentage of variations (r^2, ME; model efficiency) in observed $V_{c,max25}$ (μmol CO_2 m^{-2} s^{-1}) explained by modeled $V_{c,max25}$ (a; herbaceous, b; shrubs, c; trees) and in observed J_{max25} (μmol electron m^{-2} s^{-1}) explained by modeled J_{max25} (d; herbaceous, e; shrubs, f; trees) for different plant functional types (PFTs). The nitrogen allocation model was run with the environmental variables, leaf mass per leaf area, and the leaf nitrogen contents by using TRF1. TRF1 was a temperature response function that considered the potential for acclimation to growth temperature. The r^2 is derived by a linear regression between observed and modeled values. The dashed line is the 1:1 line.

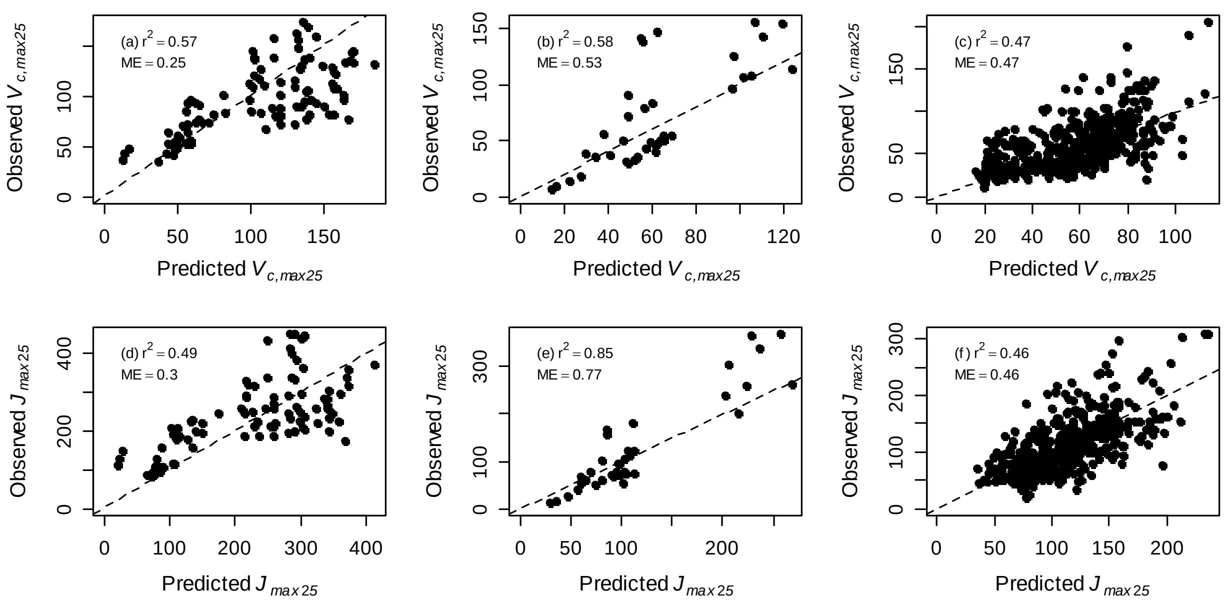

Figure S5 Percentage of variations (r^2, ME; model efficiency) in observed $V_{c,max25}$ (μmol CO_2 m^{-2} s^{-1}) explained by modeled $V_{c,max25}$ (a; herbaceous, b; shrubs, c; trees) and in observed J_{max25} (μmol electron m^{-2} s^{-1}) explained by modeled J_{max25} (d; herbaceous, e; shrubs, f; trees) for different plant functional types (PFTs). The nitrogen allocation model was run with the environmental variables, leaf mass per leaf area, and the leaf nitrogen contents by using TRF2. TRF2 was a temperature response function that did not consider change in temperature response coefficients to growth temperature. The r^2 is derived by a linear regression between observed and modeled values. The dashed line is the 1:1 line.

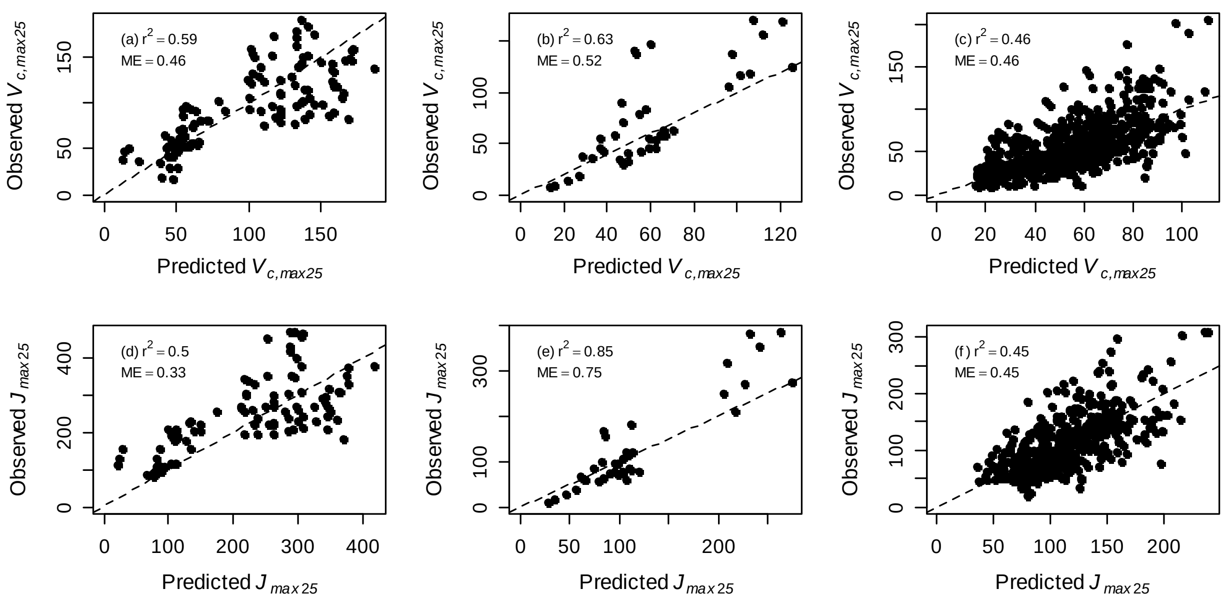

Figure S6 Summer season photosynthetic capacity for the top leaf layer in the canopy ($V_{c,max25}$; μmol CO_2 m^{-2} s^{-1} (a), J_{max25}; μmol electron m^{-2} s^{-1} (c)) under historical climatic conditions and the difference in either $V_{c,max25}$ (b) or J_{max25} (d) due to changed climatic conditions. Difference in the photosynthetic capacity was calculated as that under future climate minus that under historical climate. Ten-year monthly averages of climatic conditions for historical (1995 – 2004) and future (2090-2099) were considered. The model was run by using TRF2, which did not consider change in temperature response coefficients to growth temperature.

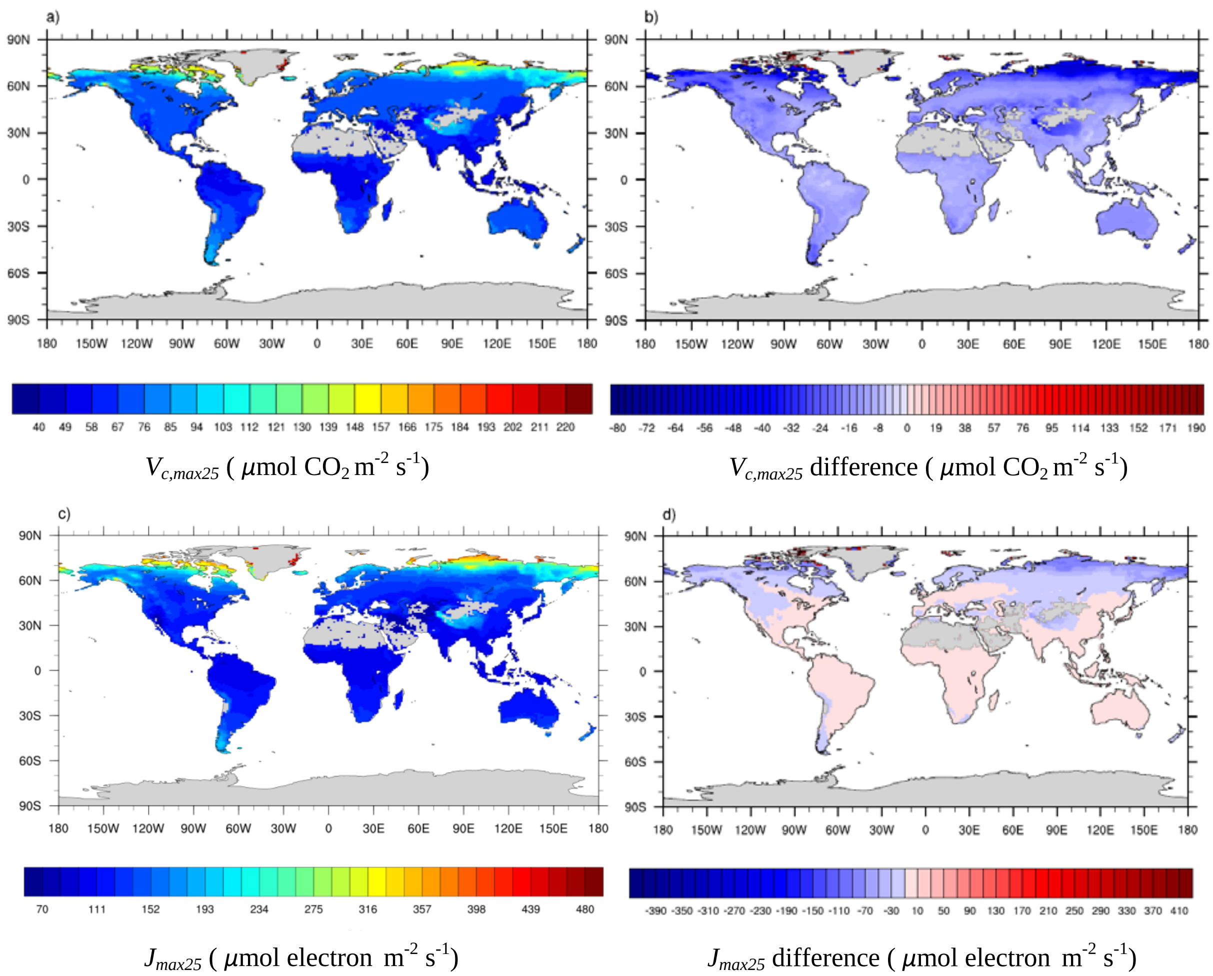

Figure S7 Sensitivity of $V_{c,max25}$ (μmol CO_2 m^{-2} s^{-1}) to changes in environmental variables (a; Temperature, b; Radiation, c; Humidity, and d; CO_2) in different regions by using TRF2. TRF2 was a temperature response function that did not consider change in temperature response coefficients to growth temperature.

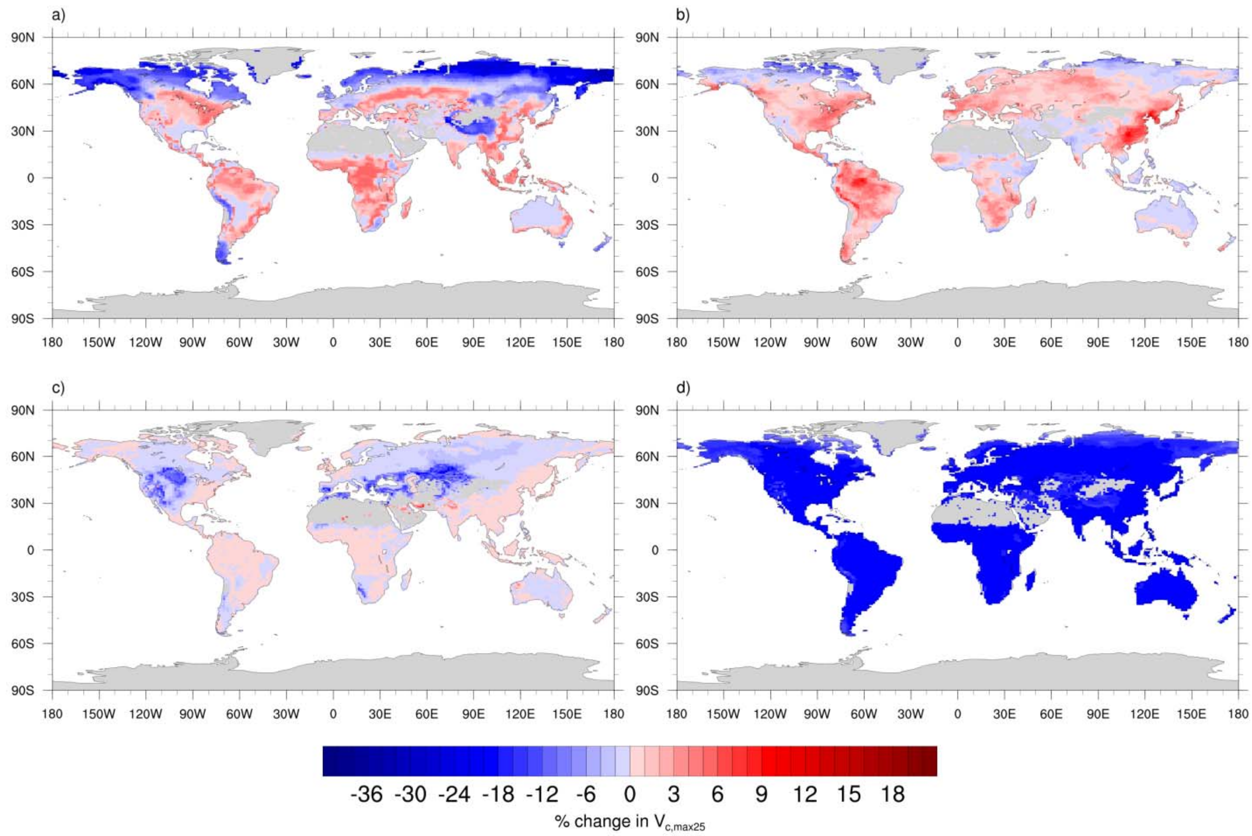

Figure S8 Sensitivity of J_{max25} (μmol electron m^{-2} s^{-1}) to changes in environmental variables (a; Temperature, b; Radiation, c; Humidity, and d; CO_2) in different regions using TRF2. TRF2 was a temperature response function that did not consider change in temperature response coefficients to growth temperature.

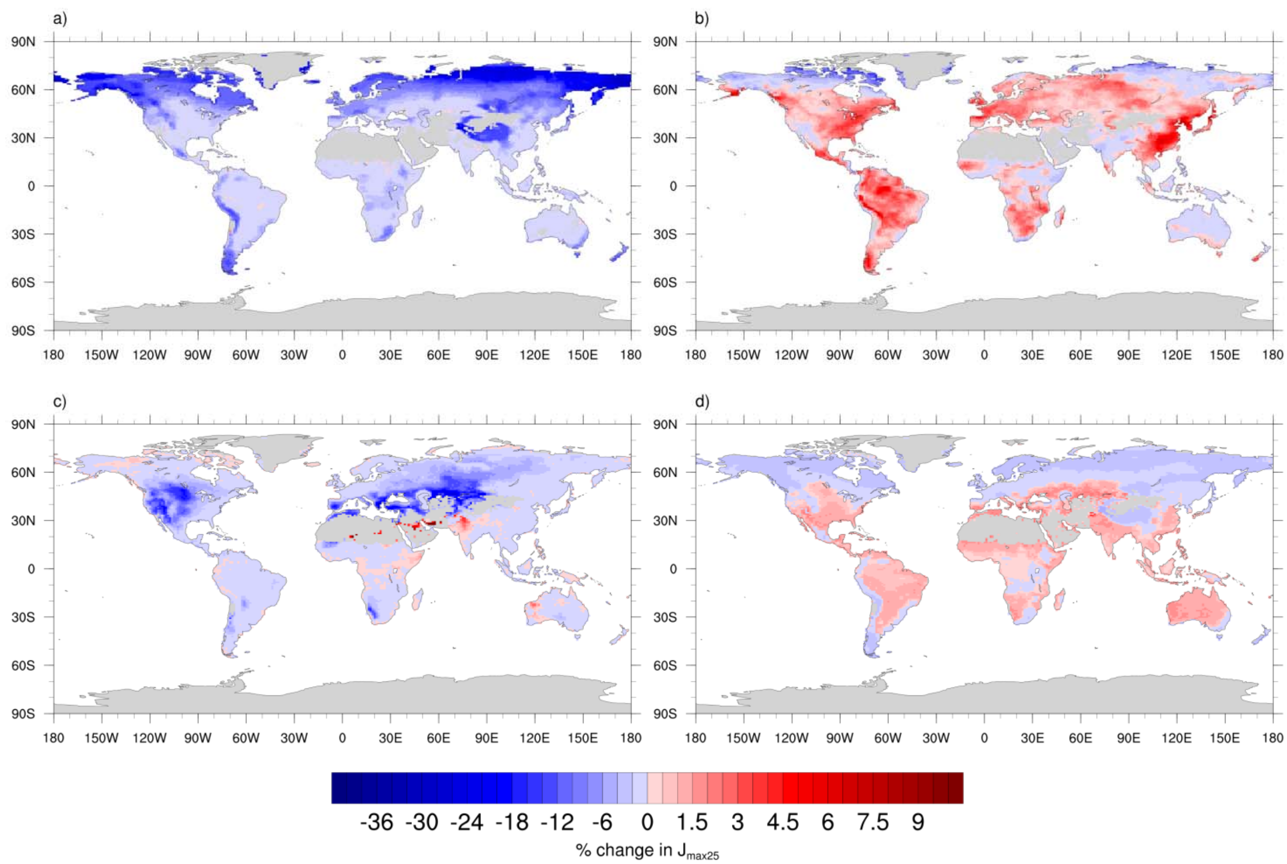

Figure S9 Summer season temperature (°C) under historical climatic conditions (a) and future climatic conditions (b). Ten-year monthly averages of temperature for historical (1995 – 2004) and future (2090-2099) predicted by CCSM 4.0 under emission scenario RCP8.5 were considered.

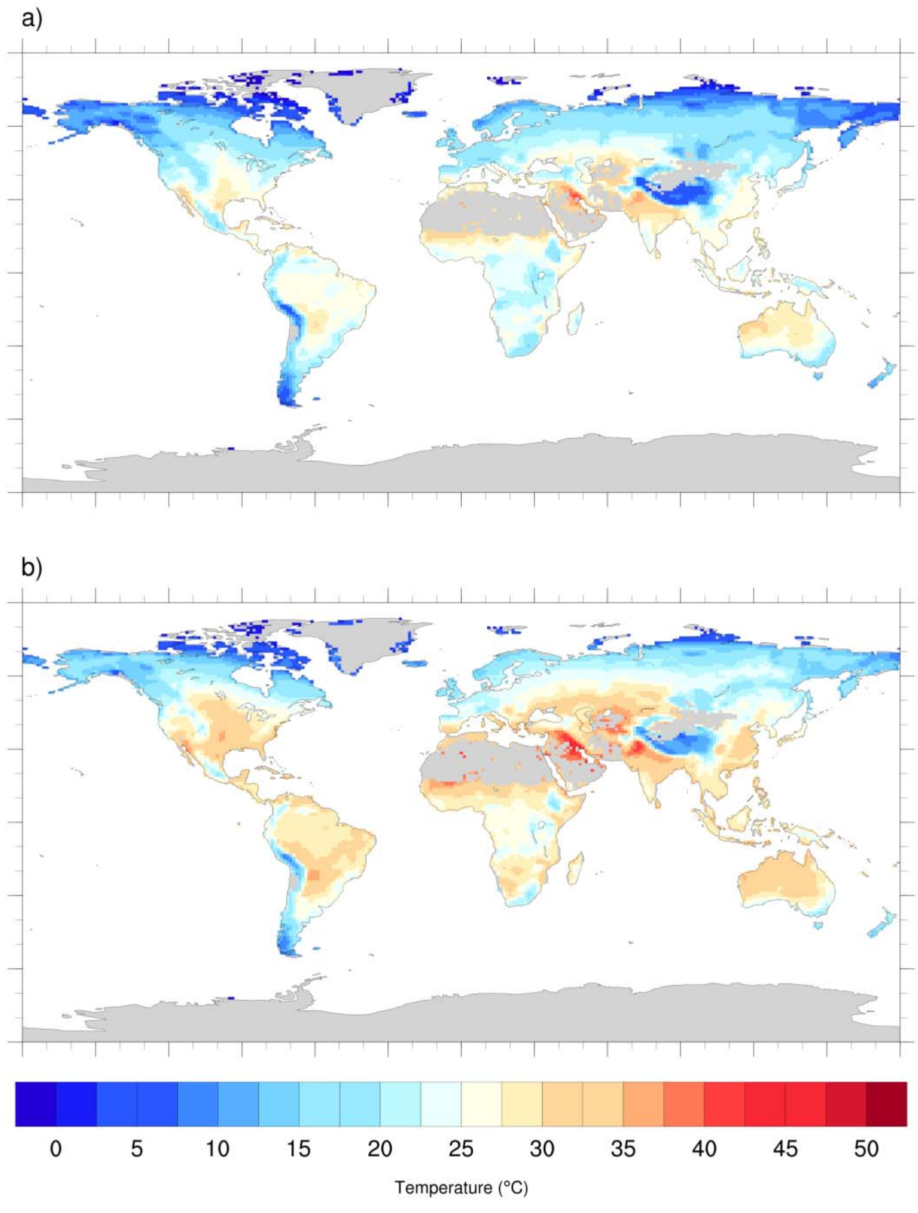

Figure S10 Summer season difference in the temperature (°C) due to changed climatic conditions (temperature under future climate minus temperature under historical climate). Ten-year monthly averages of temperature for historical (1995 – 2004) and future (2090-2099) predicted by CCSM 4.0 under emission scenario RCP8.5 were considered.

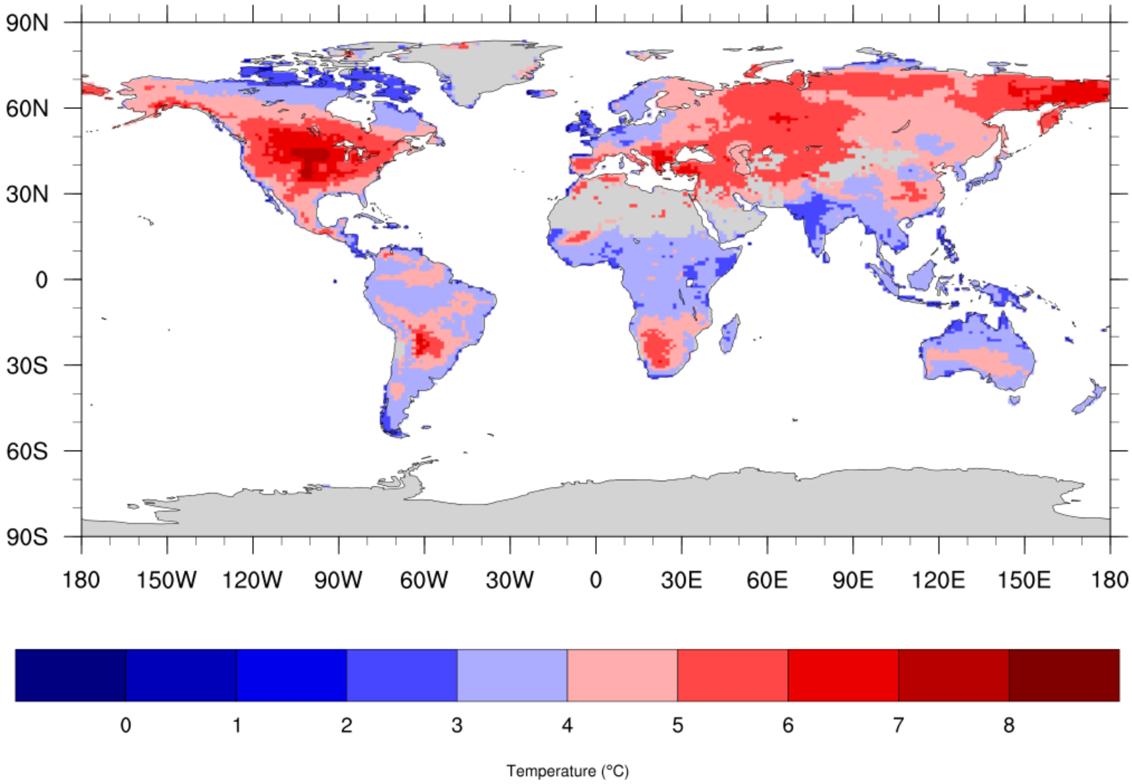

Figure S11 Summer season radiation (Radiation; W m^{-2}) under historical climatic conditions (a) and future climatic conditions (b). Ten-year monthly averages of radiation for historical (1995 – 2004) and future (2090-2099) predicted by CCSM 4.0 under emission scenario RCP8.5 were considered.

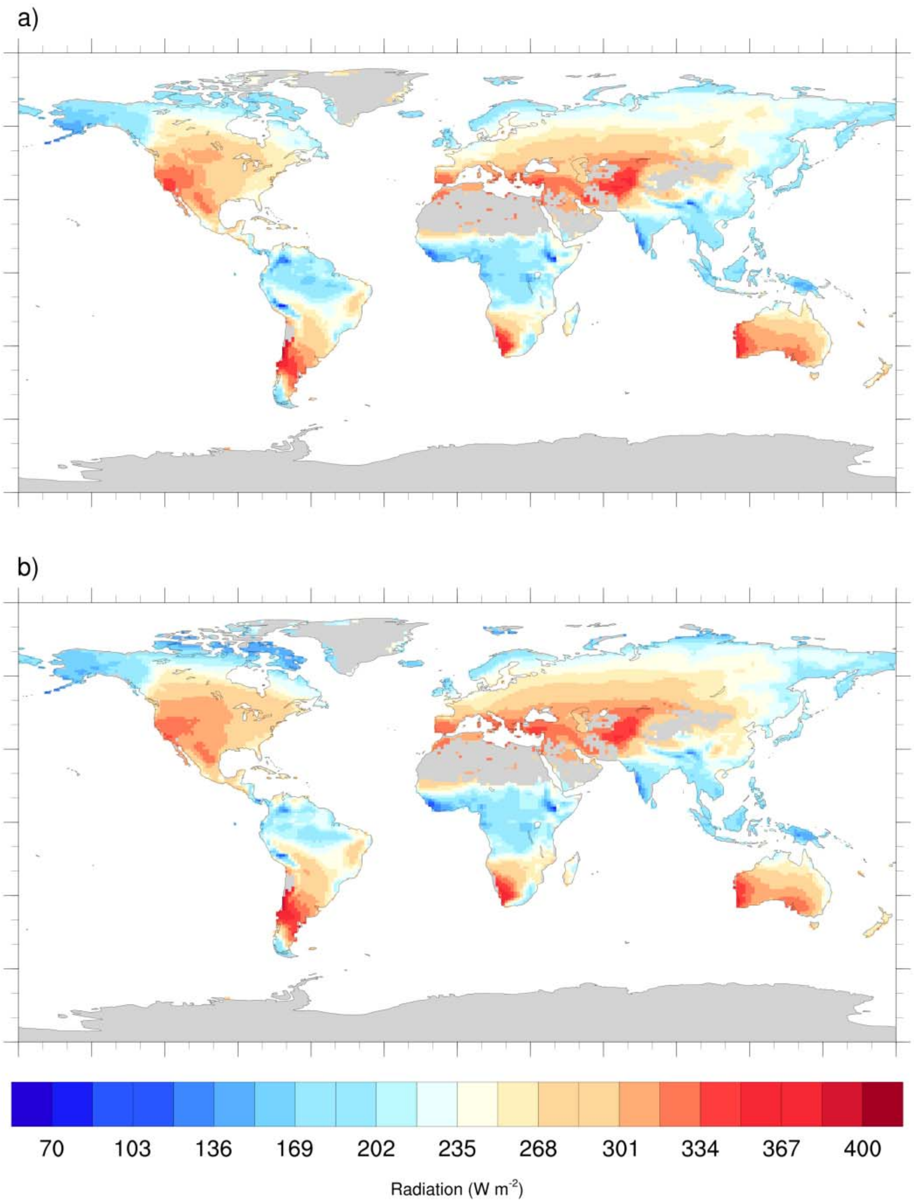

Figure S12 Summer season difference in solar radiation (W m^{-2}) due to changed climatic conditions (radiation under future climate minus radiation under historical climate). Ten-year monthly averages of radiation for historical (1995 – 2004) and future (2090-2099) predicted by CCSM 4.0 under emission scenario RCP8.5 were considered.

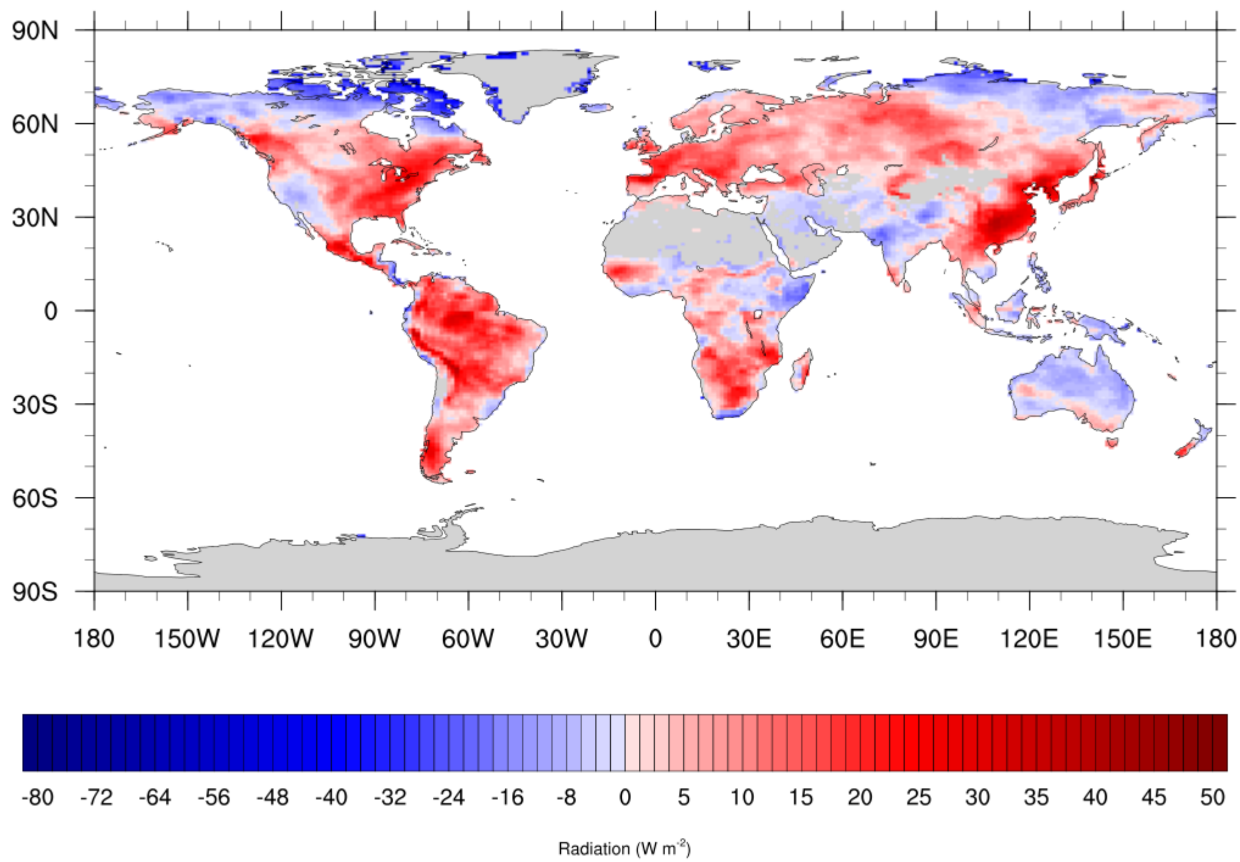

Figure S13 Summer season relative humidity (Relative Humidity; unitless) under historical climatic conditions (a) and future climatic conditions (b). Ten-year monthly averages of relative humidity for historical (1995 – 2004) and future (2090-2099) predicted by CCSM 4.0 under emission scenario RCP8.5 were considered.

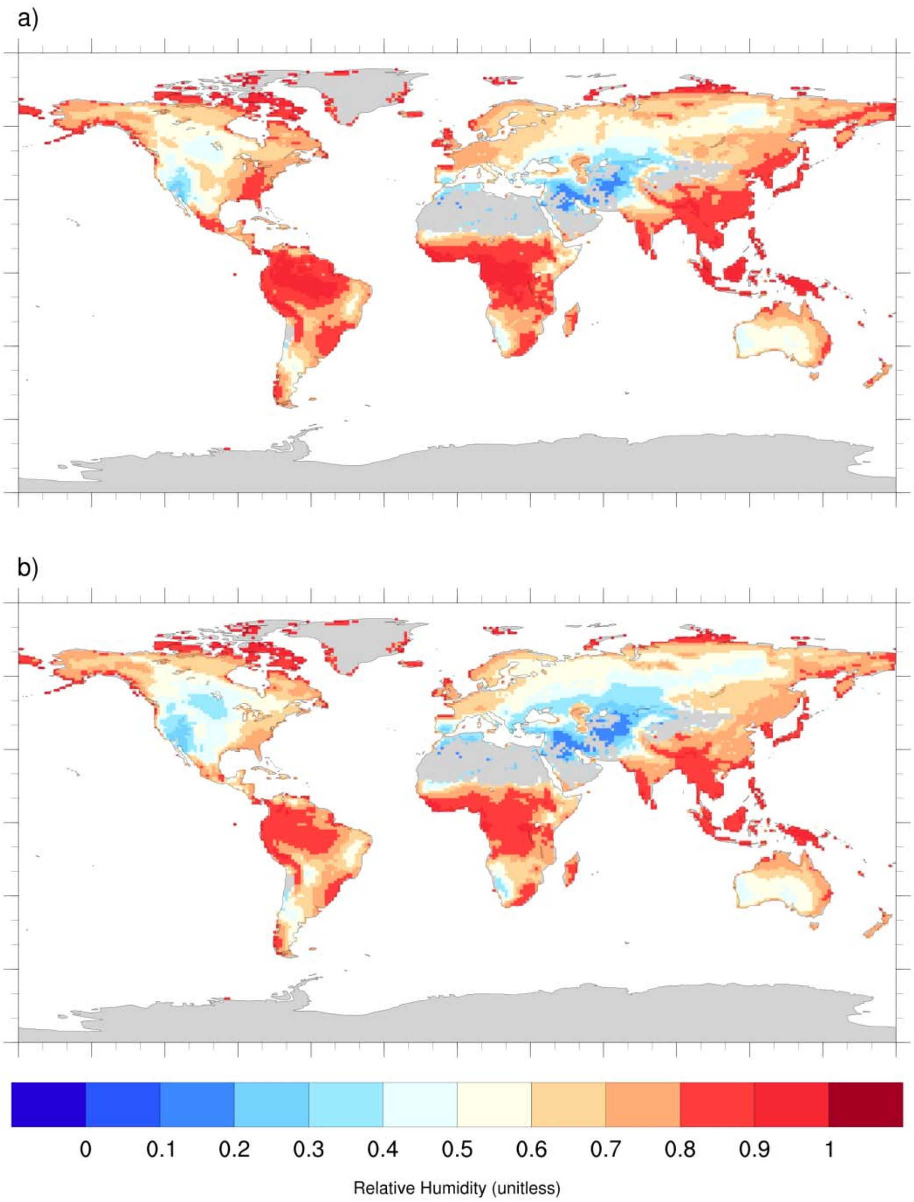

Figure S14 Summer season difference in relative humidity due to changed climatic conditions (relative humidity under future climate minus relative humidity under historical climate). Ten-year monthly averages of relative humidity for historical (1995 – 2004) and future (2090-2099) predicted by CCSM 4.0 under emission scenario RCP8.5 were considered.